Available online at www.sciencedirect.com
SCIENCE DIRECT®
Journal of Nuclear Materials 320 (2003) 292–298
journal of nuclear materials
www.elsevier.com/locate/jnucmat

Chemical thermodynamic representation of AmO_{2-x}

C. Thiriet *, R.J.M. Konings

European Commission, Joint Research Centre, Institute for Transuranium Elements, P.O. Box 2340, 76125 Karlsruhe, Germany

Received 29 January 2003; accepted 13 March 2003

Abstract

The AmO_{2-x} solid solution data set for the dependence of the oxygen potential on the composition, x, and temperature was retrieved from the literature and represented by a thermodynamic model. The data set was analysed by least-squares using equations derived from the classical thermodynamic theory for the solid solution of a solute in a solvent. Two representations of the AmO_{2-x} data were used, namely the $Am_{5/4}O_2$–AmO_2 and $AmO_{3/2}$–AmO_2 solid solution. No significant difference was found between the two, and the $Am_{5/4}O_2$–AmO_2 solution was preferred on the basis of the phase diagram. From the results the Gibbs energy of formation of $Am_{5/4}O_2$ has been derived.

1. Introduction

Within the framework of the studies on nuclear waste transmutation, it is important to study the chemical thermodynamic properties (among others) of the minor actinides compounds. The minor actinides oxides as composites with MgO or solid solutions with UO_2 or stabilized ZrO_2 are considered as fuels for transmutation. Unfortunately, few experimental results concerning AmO_{2-x} were published up to now, the high-temperature data being restricted to pressure–temperature–composition ($p^*_{O_2}$–T–x) data. $p^*_{O_2}$ is the oxygen partial pressure equal to $p(O_2)/p^0$ where p^0 is the standard pressure (10^5 Pa). In this paper we will present a thermodynamic analysis for these data, which is based on the model proposed by Lindemer and Besmann [1–4]. It assumes that the chemical potential in the fluorite-structure phase can be described as a solution of two or more species. The solvent species is chosen to have the stoichiometry of the undefected phase, in our case AmO_2. The solute species, written as Am_aO_b, is chosen to reflect with the solvent, the oxygen potential–temperature–composition behaviour and the system phase relations. The goal of the present work is to determine the best expression of solute species by applying the thermodynamic model proposed by Lindemer and Besmann to describe the thermodynamic behaviour of AmO_{2-x}.

2. The Am–O phase diagram

The available information for the Am–O system is restricted to the experimental studies by Sari and Zamorani [5] using thermal and ceramographic analysis and by Chikalla and Turcotte [6], Chikalla and Eyring [7,8] and Casalta [9] using oxygen potential measurements. In addition to AmO_2, the following phases have been identified in these studies:

- α, α_1, α_2: substoichiometric fcc AmO_{2-x} phase,
- A: hexagonal phase Am_2O_3,
- C: cubic phase Am_2O_3 at low temperature,
- C′: cubic phase $AmO_{1.5+x}$ at elevated, intermediate temperature.

However, the experimental results are restricted to the lower temperature range ($T < 1673$ K) and are not conclusive. The results of Sari and Zamorani [5] and Casalta [9], which both cover the range between $AmO_{1.5}$ and AmO_2, indicate differences at the $AmO_{1.5}$ side of the

* Corresponding author. Tel.: +49-7247 951246; fax: +49-7247 951590.
E-mail address: catherine.thiriet@itu.fzk.de (C. Thiriet).

0022-3115/03/$ - see front matter © 2003 Elsevier B.V. All rights reserved.
doi:10.1016/S0022-3115(03)00188-0

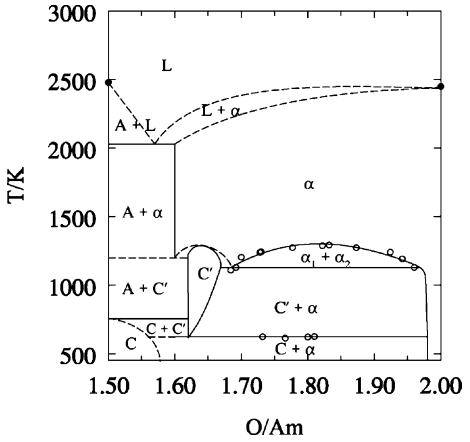

Fig. 1. The tentative americium–oxygen phase diagram in the region $AmO_{1.5}$–AmO_2; α, α_1, α_2: substoichiometric fcc AmO_{2-x} phase; A: hexagonal phase Am_2O_3; C: cubic phase Am_2O_3 at low temperature; C′: cubic phase $AmO_{1.5+x}$ at high temperature; (o) experimental data from [5].

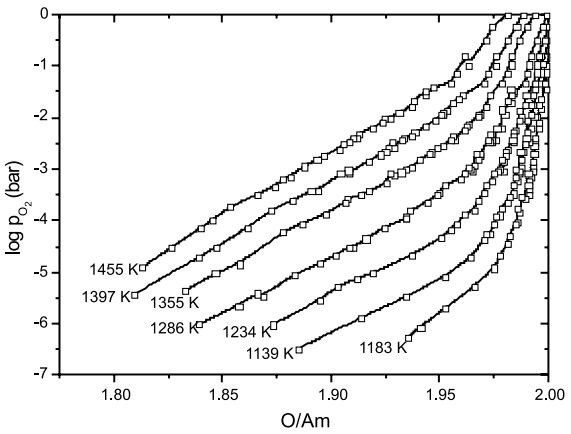

Fig. 2. Experimental dissociation pressure isotherms [7].

diagram with respect to the stability of hexagonal Am_2O_3.

The melting behaviour in the high-temperature region of the $AmO_{1.5}$–AmO_2 system has been estimated by Zhang et al. [10] based on phase diagram calculations assuming similar behaviour to the Pu–O and Ln–O systems, and re-interpretation of the melting study of AmO_2 with different heating rates by McHenry [11].

A number of phase diagrams have been proposed on the basis of this information [12–15], none of them being fully correct with respect to the phase rule. For example, the phase boundary of C′ is in all cases wrong, and the simple combination of the calculated diagrams for the $AmO_{1.5}$–$AmO_{1.62}$ and $AmO_{1.62}$–AmO_2 regions by Zhang et al. [10], as done in [15], leads to an incorrect result. A tentative phase diagram that is consistent with the phase rule is shown in Fig. 1. It should be realized, however, that the phase boundary of the C phase as well as the high-temperature range are highly speculative.

3. The representation of AmO_{2-x}

We considered the data points of oxygen potential–temperature–composition for AmO_{2-x} measured by Chikalla and Eyring [7]. The data by Casalta [9] are in reasonable agreement but are not used in our treatment since they are mainly made in the region of the miscibility gap and are limited in number. The results of Chikalla and Eyring [7] comprise 283 data points which have been determined by a thermogravimetric isopiestic technique. The temperature and pressure ranges investigated were 1139–1445 K and from 10^{-6} to 1 bar oxygen, respectively. The nonstoichiometric compositions encountered under these conditions covered the interval $1.80 < O/Am < 2.00$ (Fig. 2). The data points have been extracted from the graph in [7] using a digital technique.

The fluorite-structure AmO_{2-x} is taken to be a solution of the solvent end member AmO_2 and a lower oxide solute species Am_aO_b, also having the fluorite structure. Assuming that AmO_{2-x} is a solution of the two oxides species with a constant energy of interaction allows the standard Gibbs energy of formation of the phase to be expressed as

$$\begin{aligned}\Delta_f G^0(AmO_{2-x}) = {} & \frac{n_{AmO_2}}{n}\Delta_f G^0(AmO_2) \\ & + \frac{n_{Am_aO_b}}{n}\Delta_f G^0(Am_aO_b) \\ & + \frac{n_{AmO_2}}{n}RT\ln\left(\frac{n_{AmO_2}}{n}\right) \\ & + \frac{n_{Am_aO_b}}{n}RT\ln\left(\frac{n_{Am_aO_b}}{n}\right) \\ & + \frac{n_{AmO_2}}{n_{Am_aO_b}}n^2E \end{aligned} \quad (1)$$

with $\Delta_f G^0(i)$ standard Gibbs energy of formation of phase i, n_i moles of species i, n sum of the moles of the species, R ideal gas constant, T absolute temperature, E energy of interaction between solvent and solute. The moles, n, of each species in the solution are calculated from the mass-balance equations for americium and oxygen, respectively:

$$1 = n_{AmO_2} + a n_{Am_aO_b},$$

$$O/M = 2 - x = 2n_{AmO_2} + b n_{Am_aO_b}$$

and thus it follows that

$$\begin{aligned} n_{Am_aO_b} &= \frac{x}{2a-b}, \\ n_{AmO_2} &= 1 - \frac{ax}{2a-b}. \end{aligned} \quad (2)$$

The partial molar Gibbs energies for each of the solution components are defined as

$$\Delta\overline{G}(\mathrm{AmO_2}) = \frac{\partial(n\Delta_f G^0(\mathrm{AmO_{2-x}}))}{\partial n_{\mathrm{AmO_2}}},$$
$$\Delta\overline{G}(\mathrm{Am_aO_b}) = \frac{\partial(n\Delta_f G^0(\mathrm{AmO_{2-x}}))}{\partial n_{\mathrm{Am_aO_b}}}. \quad (3)$$

From (1)–(3), it follows:

$$\Delta\overline{G}(\mathrm{AmO_2}) = \Delta_f G^0(\mathrm{AmO_2}) + RT\ln\left(\frac{2a-b-ax}{2a-b+x(1-a)}\right) + \left(\frac{x}{2a-b+x(1-a)}\right)^2 E,$$
$$\Delta\overline{G}(\mathrm{Am_aO_b}) = \Delta_f G^0(\mathrm{Am_aO_b}) + RT\ln\left(\frac{x}{2a-b+x(1-a)}\right) + \left(\frac{2a-b-ax}{2a-b+x(1-a)}\right)^2 E. \quad (4)$$

The component species of $\mathrm{AmO_{2-x}}$ must relate the oxygen potential–temperature–composition data set to the unknown values of a, b, E according to the reaction:

$$\frac{2}{2a-b}\mathrm{Am_aO_b} + \mathrm{O_2} \rightleftarrows \frac{2a}{2a-b}\mathrm{AmO_2} \quad (5)$$

The equilibrium partial molar Gibbs energies relation for the reaction (5) can be written as

$$\frac{2a}{2a-b}\Delta\overline{G}(\mathrm{AmO_2}) - \frac{2}{2a-b}\Delta\overline{G}(\mathrm{Am_aO_b}) - \Delta\overline{G}(\mathrm{O_2}) = 0 \quad (6)$$

with

$$\Delta\overline{G}(\mathrm{O_2}) = RT\ln\left(\frac{p(\mathrm{O_2})}{p^0}\right) = RT\ln p^*_{\mathrm{O_2}}.$$

Combining (4) with the standard formula for the Gibbs energy of reaction

$$\Delta_r G^0 = \Delta_r H^0 - T\Delta_r S^0 = \frac{2a}{2a-b}\Delta_f G^0(\mathrm{AmO_2}) - \frac{2}{2a-b}\Delta_f G^0(\mathrm{Am_aO_b})$$

it follows that

$$\Delta_r H^0 - T\Delta_r S^0 - RT\ln p^*_{\mathrm{O_2}} = \frac{2}{2a-b}RT\ln\left[\frac{x(x(1-a)+2a-b)^{a-1}}{(2a-b-ax)^a}\right] + \frac{2}{2a-b}\frac{(2a-b-ax)^2 - ax^2}{(2a-b+x(1-a))^2}E. \quad (7)$$

The interaction energy is assumed to equal:

$$E = \Delta^E H - T\Delta^E S. \quad (8)$$

From (7) and (8) it finally follows that

$$\ln p^*_{\mathrm{O_2}} = \frac{\Delta_r H^0}{RT} - \frac{\Delta_r S^0}{R} - \frac{2}{2a-b}\ln\left[\frac{x(x(1-a)+2a-b)^{a-1}}{(2a-b-ax)^a}\right] + \frac{2}{2a-b}\frac{(2a-b-ax)^2 - ax^2}{(2a-b+x(1-a))^2}\left(\frac{\Delta^E H - T\Delta^E S}{RT}\right). \quad (9)$$

4. Analysis of the data for $\mathrm{AmO_{2-x}}$

It has been determined that equations relating T, $p^*_{\mathrm{O_2}}$ and x from the current methodology can be reduced to the simple expression, as explained in [1]:

$$\ln(p^*_{\mathrm{O_2}}) = A/T + B - s\ln(x), \quad (10)$$

where s replaces the coefficient $2/(2a-b)$. Least-squares analysis of the data permitted the determination of s which is the absolute value of the slope of the $\ln(x) - \ln(p^*_{\mathrm{O_2}})$ plot at constant temperature. The T, $p^*_{\mathrm{O_2}}$, x values located outside the miscibility gap ($\alpha_1 + \alpha_2$) are considered because too few data exist to try to reproduce this domain of the phase diagram. The analysis of the approximately 280 data gave a slope between 3.53 and 4.34. Since s must be an integer, it is taken to equal 4. With this value of s, the chemical formula of the solute species is determined as we will discuss below. The choice for this species was also done in coherence with the phase diagram shown in Fig. 1.

4.1. AmO_2–$Am_{5/4}O_2$ solution

First, b/a equal to 1.6 has been analysed because this ratio corresponds to a defined compound in the temperature and composition range (Fig. 1). The only chemical formula for the solute species which is consistent with this ratio as well as with $s = 2/(2a-b) = 4$ was found to be $\mathrm{Am_{5/4}O_2}$ (O/Am = 1.6). Thus it follows that $a = \frac{5}{4}$ and $b = 2$.

This compound is used to quantitatively describe $\mathrm{AmO_{2-x}}$, with the thermodynamic parameters determined by fitting to the oxygen potential–temperature–composition data set. By replacing a and b, the equilibrium reaction from Eqs. (5) and (7) becomes

$$4\mathrm{Am_{5/4}O_2} + \mathrm{O_2} \rightleftarrows 5\mathrm{AmO_2} \quad (11)$$

$$\Delta_r H^0 - T\Delta_r S^0 - RT\ln p^*_{\mathrm{O_2}} = 4RT\ln\left[\frac{x(1/2-x/4)^{1/4}}{(1/2-5x/4)^{5/4}}\right] + \frac{4(5x^2-20x+4)}{(2-x)^2}(\Delta^E H - T\Delta^E S). \quad (12)$$

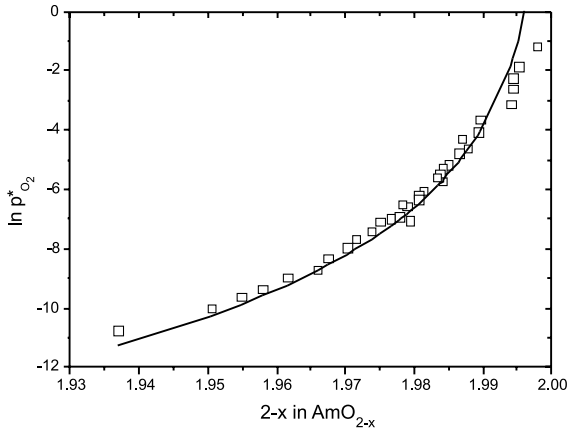

Fig. 3. Least-squares fit (—) with the relation given of the oxygen potential–temperature–composition data (□) at 1234 K.

Finally, Eq. (9) is written as

$$\ln p^*_{O_2} = \frac{\Delta_r H^0}{RT} - \frac{\Delta_r S^0}{R} - 4\ln\left[\frac{x(1/2-x/4)^{1/4}}{(1/2-5x/4)^{5/4}}\right] - 4\left(\frac{\Delta_e H - T\Delta^E S}{RT}\right)\left(\frac{5x^2-20x+4}{(2-x)^2}\right). \quad (13)$$

A least-squares fit of the oxygen potential–temperature–composition data (Fig. 3) to Eq. (13) provides the values of $\Delta_r H^0$, $\Delta_r S^0$, $\Delta^E H$ and $\Delta^E S$.

The same procedure was applied for the oxygen potential–temperature- composition data at each temperature. Fig. 4 includes the values of model parameters found as a function of the temperature.

Note that the $\Delta_r H^0$ parameter was found to be linearly dependent on the temperature. Only the $\Delta_r H$ value at 1183 K was found to deviate significantly ($>2\sigma$) from the trend and was therefore not retained for the linear fit of $\Delta_r H$ vs temperature. The values of the thermodynamic parameters thus obtained are listed in Table 1.

The oxygen potential–temperature–composition behaviour of AmO_{2-x} can now be expressed as

$$RT\ln p^*_{O_2} = (-190\,312 - 302T) + 344.1T - 4RT\ln\left[\frac{x(1/2-x/4)^{1/4}}{(1/2-5x/4)^{5/4}}\right] - 4(87\,573 - 59.3T)\left(\frac{5x^2-20x+4}{(2-x)^2}\right)$$

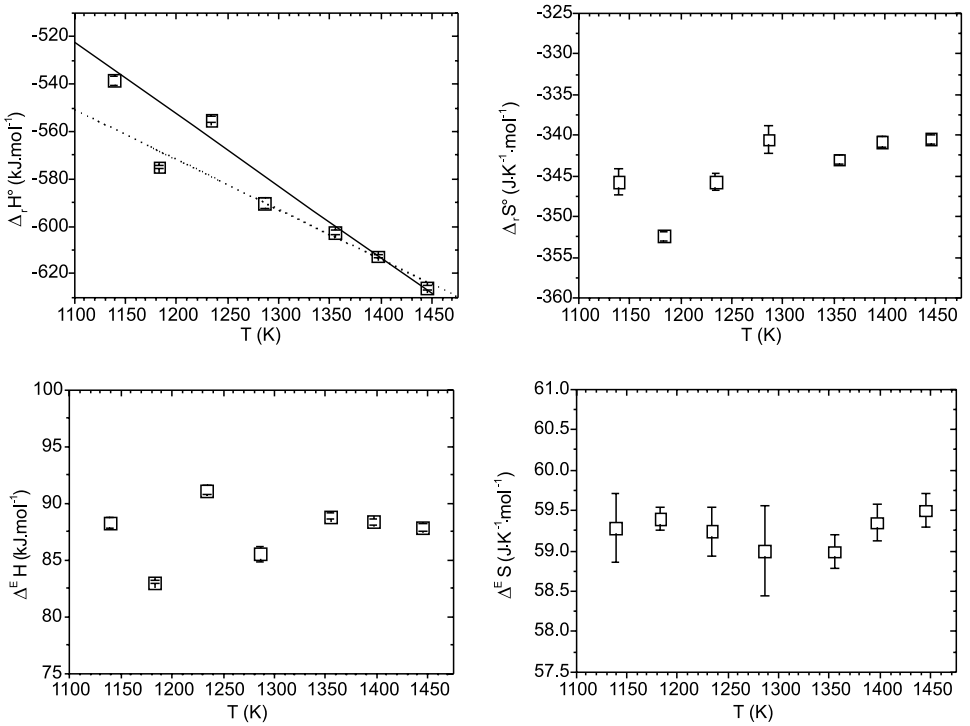

Fig. 4. Representation of AmO_{2-x} model parameters from the fit of the oxygen potential–temperature–composition data set; (—) fit of $\Delta_r H^0$ values without value at 1183 K; (···) fit of $\Delta_r H^0$ values with value at 1183 K.

Table 1
AmO_{2-x} model parameters from the fit of the oxygen potential–temperature–composition data set

Thermodynamic parameters	$Am_{5/4}O_2$ b/a ratio = 1.6		$AmO_{3/2}$ b/a ratio = 1.5		Units
$\Delta_r H^0$	−190 312	−302 T	−165 371	−332 T	($J\,mol^{-1}$)
$\Delta_r S^0$	−344.1	±4.3	−344.0	±0.7	($J\,K^{-1}\,mol^{-1}$)
$\Delta^E H$	87 573	±2596	85 171	±2071	($J\,mol^{-1}$)
$\Delta^E S$	59.3	±0.2	59.3	±0.4	($J^{-1}\,mol^{-1}$)

with

$$\begin{aligned}
&\Delta_r H^0 = -190\,312 - 302T \ (\mathrm{J\,mol^{-1}}),\\
&\Delta_r S^0 = -344.1 \pm 4.3 \ (\mathrm{J\,K^{-1}\,mol^{-1}}),\\
&\Delta^E H^0 = 87\,573 \pm 2596 \ (\mathrm{J\,mol^{-1}}),\\
&\Delta^E S^0 = 59.3 \pm 0.2 \ (\mathrm{J\,K^{-1}\,mol^{-1}}).
\end{aligned} \tag{14}$$

Fig. 5 shows the good agreement between Eq. (14) and the experimental data. Fig. 6 shows the residuals as a function of $\ln(x)$.

4.2. AmO_2–$AmO_{3/2}$ solution

The choice of b/a equal to 1.5 has also been considered as it corresponds to the well-known sesquioxide phase. The Am_aO_b species considered are $AmO_{3/2}$, $Am_{4/3}O_2$ and Am_3O_2, but only the species $AmO_{3/2}$ fulfills Eq. (5). This formula with AmO_2 has been used to quantitatively describe AmO_{2-x} in the same way as described in the previous section. With $a = 1$ and $b = \frac{3}{2}$, the equilibrium reaction from Eqs. (5) and (9) becomes

$$4AmO_{3/2} + O_2 \rightleftarrows 4AmO_2 \tag{15}$$

$$\begin{aligned}
\ln p^*_{O_2} = {} & \frac{\Delta_r H^0}{RT} - \frac{\Delta_r S^0}{R} - 4\ln\left(\frac{2x}{1-2x}\right)\\
& - \frac{4(1-4x)}{RT}(\Delta^E H - T\Delta^E S).
\end{aligned} \tag{16}$$

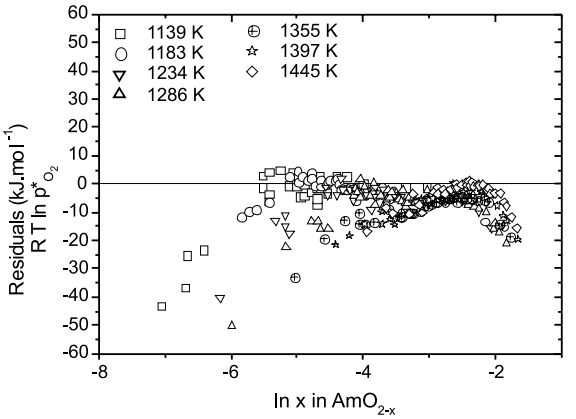

Fig. 6. Residuals plotted vs $\ln(x)$ for solute species $Am_{5/4}O_2$.

The values of $\Delta_r H^0$, $\Delta_r S^0$, $\Delta^E H$ and $\Delta^E S$ derived for the oxygen potential–temperature–composition data by least-squares fit to Eq. (16), are listed in Table 1.

It should be noted that $\Delta_r H^0$ was found to depend on the temperature also in this case and that the data at 1183 K have not been considered. The oxygen potential–temperature–composition behaviour of AmO_{2-x} can be described using these parameters as

$$\begin{aligned}
RT\ln p^*_{O_2} = {} & (-165\,371 - 332T) + 344.0T - 4RT\\
& \times \ln\left(\frac{2x}{1-2x}\right) - 4(85\,171 - 59.3T)(1-4x)
\end{aligned}$$

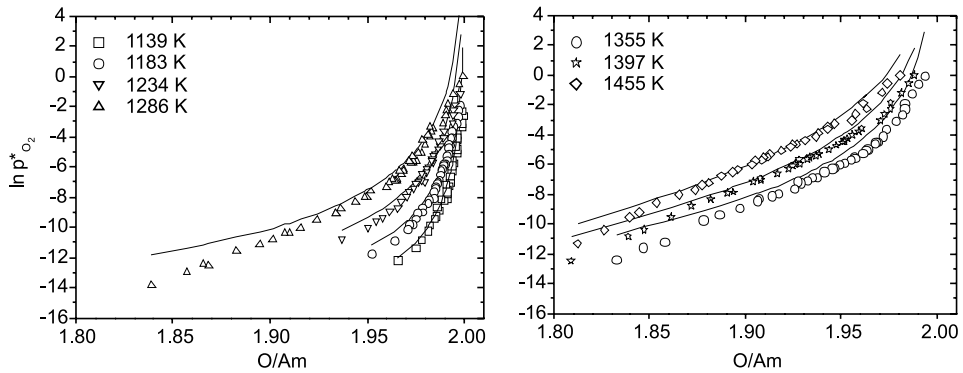

Fig. 5. Dependence of $\ln p^*_{O_2}$ on O/Am for our relation.

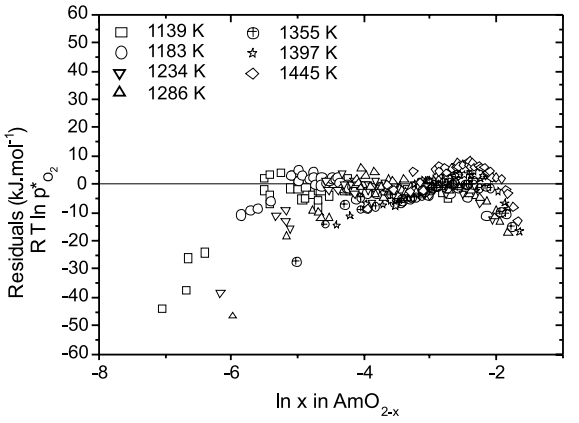

Fig. 7. Residuals plotted vs $\ln(x)$ for the solute species $AmO_{3/2}$.

Table 2
Comparison of mean residuals between both for the two models described in the text

Temperature (K)	$Am_{5/4}O_2$	$AmO_{3/2}$
1139	-4.4 ± 10.5	-4.9 ± 10.6
1183	-2.2 ± 4.0	-4.0 ± 7.0
1234	-6.35 ± 7.0	-1.4 ± 3.9
1286	-9.9 ± 16.3	-6.1 ± 16.3
1355	-9.6 ± 5.6	-4.1 ± 5.6
1397	-6.8 ± 5.5	-0.5 ± 5.7
1455	-4.1 ± 4.7	2.8 ± 5.2

with

$$\begin{aligned}
&\Delta_r H^0 = -165\,371 - 332T \ (\mathrm{J\,mol^{-1}}),\\
&\Delta_r S^0 = -344.0 \pm 0.7 \ (\mathrm{J\,K^{-1}\,mol^{-1}}),\\
&\Delta^E H^0 = 85\,171 \pm 2071 \ (\mathrm{J\,mol^{-1}}),\\
&\Delta^E S^0 = 59.3 \pm 0.4 \ (\mathrm{J\,K^{-1}\,mol^{-1}}).
\end{aligned} \tag{17}$$

The comparison between the model and the experimental data is similar as in the AmO_2–$Am_{5/4}O_2$ case, and is shown in Fig. 7. The average of the residuals, however, shows that the second model using the formula $AmO_{3/2}$ reproduces statistically somewhat better the oxygen potential–temperature–composition behaviour of AmO_{2-x} (Table 2).

5. Discussion

Lindemer and Bessmann, who first proposed this thermodynamic model, used the ratio $b/a = 1.5$ for the description of CeO_{2-x} [4] and PuO_{2-x} [1]. The comparison of these systems with AmO_{2-x} is justified since the phase diagrams for the O–Pu [16] O–Ce [17], and O–Am systems are similar. The analysis for $b/a = 1.5$, corresponding to the sesquioxide, reproduces the potential–temperature–composition data for AmO_{2-x} statistically somewhat better than $b/a = 1.6$. However, the latter ratio seems more logical on the basis the phase diagram, as it is the end composition of the AmO_{2-x} phase. Taking into account that the difference between the two models is small, we prefer the solute species $Am_{5/4}O_2$.

From the thermodynamic parameters shown in Table 1, the standard Gibbs energy of formation of the $Am_{5/4}O_2$ solute species can thus be determined. Based on the present results we can write

$$\Delta_r G^0 = \Delta_r H^0 - T\Delta_r S^0 = -190\,312 + 42.1T \tag{18}$$

and

$$\begin{aligned}
\Delta_r G^0 &= \frac{2a}{2a-b}\Delta_f G^0(\mathrm{AmO_2}) - \frac{2}{2a-b}\Delta_f G^0(\mathrm{Am_aO_b})\\
&= 5\Delta_f G^0(\mathrm{AmO_2}) - 4\Delta_f G^0(\mathrm{Am_{5/4}O_2}).
\end{aligned} \tag{19}$$

The standard Gibbs energy of formation of AmO_2 is calculated from data in Appendix A, which give for the relevant temperature region between 1100 and 1500 K:

$$\Delta_f G^0(\mathrm{AmO_2}) = -924\,068 + 167.47T \ (\mathrm{J\,mol^{-1}}). \tag{20}$$

For the solute species, Eqs. (18)–(20) lead to

$$\Delta_f G^0(\mathrm{Am_{5/4}O_2}) = -1\,107\,507 + 198.81T \ (\mathrm{J\,mol^{-1}}). \tag{21}$$

With Eqs. (4), (20), and (21), the partial molar Gibbs energies are

$$\begin{aligned}
\Delta\overline{G}(\mathrm{AmO_2}) &= (-924\,068 + 167.47T) + RT\ln\left(\frac{2-5x}{2-x}\right)\\
&\quad + \left(\frac{4x}{2-x}\right)^2(87\,573 - 59.25T),\\
\Delta\overline{G}(\mathrm{Am_{5/4}O_2}) &= (-1\,107\,507 + 198.81T) + RT\ln\left(\frac{4x}{2-x}\right)\\
&\quad + \left(\frac{2-5x}{2-x}\right)^2(87\,573 - 59.25T).
\end{aligned} \tag{22}$$

6. Conclusion

In the present paper, the feasibility has been demonstrated to describe the interdependence of the oxygen potential–composition–temperature relation for AmO_{2-x}. The representation based on an assumed equilibrium between O_2, AmO_2 and $Am_{5/4}O_2$ has been preferred to $AmO_{3/2}$ for its coherence with the Am–O phase diagram. A good agreement has been obtained between calculated and experimental values. From the thermodynamic

model the partial molar Gibbs energies, Eqs. (4) and (18)–(22) have been determined and can be used in any equilibrium calculation involving AmO_{2-x}. However, it should be taken into account that the AmO_{2-x} phase shows at low temperatures a miscibility gap for which too few data exist to be included in our analysis. Supplementary experimental data are required for this.

Acknowledgement

The authors wish to thank Dr H. Kleykamp for his advice on the Am–O phase diagram.

Appendix A. The thermodynamic properties of AmO_2 (cr)

The standard Gibbs energy of formation of AmO_2 is calculated from the heat capacity, the standard entropy and the standard enthalpy of formation of AmO_2 shown below:

$$\Delta_f H^0(\mathrm{AmO_2}, 298.15\ \mathrm{K}) = -(932.3 \pm 3.0)\ (\mathrm{kJ\,mol^{-1}}),$$

$$S^0(\mathrm{AmO_2}, 298.15\ \mathrm{K}) = 77.8 \pm 5\ (\mathrm{J\,K^{-1}\,mol^{-1}}),$$

$$C_p^0(\mathrm{AmO_2}, T) = 66.8904 + 19.1123 \times 10^{-3} T - 4.6356 \times 10^{-6} T^2 - 0.548830 \times 10^{6} T^{-2}\ (\mathrm{J\,K^{-1}\,mol^{-1}}),$$

$$C_p^0(\mathrm{AmO_2}, 298.15\ \mathrm{K}) = 66.00\ (\mathrm{J\,K^{-1}\,mol^{-1}}).$$

The enthalpy of formation is taken from the recent evaluation by Silva et al. [14] of the experimental data by Morss and Fuger [18]. The standard entropy is the estimate by Konings [19] based on a description of the entropy data for the actinide dioxides as the sum of the lattice and excess entropies, the former taken identical to ThO_2, the latter calculated from crystal field energies [20]. The heat capacity of AmO_2 has been calculated for the present work in a similar manner from the heat capacity of ThO_2 and the crystal field energies for the ground state and the excited states [20]. The entropy and the high-temperature heat capacity differ considerably from the values given by Silva et al. [14], which are based on the simple assumption that they are (almost) identical to PuO_2. It can be shown that this is not true because the crystal field energies and thus the resulting excess heat capacity of PuO_2 and AmO_2 are significantly different.

References

[1] T.M. Besmann, T.B. Lindemer, J. Nucl. Mater. 130 (1985) 489.
[2] T.B. Lindemer, T.M. Besmann, J. Nucl. Mater. 130 (1985) 473.
[3] T.M. Besmann, J. Brynestad, J. Am. Ceram. Soc. 69 (1986) 867.
[4] T.B. Lindemer, CALPHAD 10 (1986) 129.
[5] C. Sari, E. Zamorani, J. Nucl. Mater. 37 (1970) 324.
[6] T.D. Chikalla, R.P. Turcotte, NBS Special Issue 364 (1972) 319.
[7] T.D. Chikalla, L. Eyring, J. Inorg. Nucl. Chem. 29 (1967) 2281.
[8] T.D. Chikalla, L. Eyring, J. Inorg. Nucl. Chem. 30 (1968) 133.
[9] S. Casalta, PhD thesis, University Aix-Marseille I, 1996.
[10] H. Zhang, R.J.M. Konings, M.E. Huntelaar, E.H.P. Cordfunke, J. Nucl. Mater. 250 (1998) 88.
[11] R.E. McHenry, Trans. Am. Nucl. Soc. 295 (1965) 615.
[12] E.H.P. Cordfunke, R.J.M. Konings, E.F. Westrum Jr., J. Nucl. Mater. 167 (1989) 205.
[13] H. Okamoto, J. Phase Equilibria 12 (1991) 696.
[14] R.J. Silva, G. Bidoglio, M.H. Rand, P.B. Robouch, H. Wanner, I. Puigdomenech, Chemical Thermodynamics of Americium, Elsevier, 1995.
[15] R.J.M. Konings, J. Nucl. Sci. Technol. (Suppl. 3) (2002) 682.
[16] H.A. Wriedt, Bull. Alloy Phase Diagrams 11 (1990) 184.
[17] T.B. Massalski, Handbook of Binary Alloys, 2nd Ed., ASM International, Materials Park, OH, 1990, p. 1089.
[18] L.R. Morss, J. Fuger, J. Inorg. Nucl. Chem. 43 (1981) 2059.
[19] R.J.M. Konings, J. Nucl. Mater. 295 (2001) 57.
[20] J.C. Krupa, IPN Orsay France, personal communication.